 CMES, vol.102, no.3, pp.183-210, 2014

Friction and Wear Modelling in Fiber-Reinforced Composites

L. Rodríguez-Tembleque[1] and M.H. Aliabadi[2]

Abstract: This work presents new contact constitutive laws for friction and wear modelling in fiber-reinforced plastics (FRP). These laws are incorporated to a numerical methodology which allows us to solve the contact problem taking into account the anisotropic tribological properties on the interfaces. This formulation uses the Boundary Element Method for computing the elastic influence coefficients. Furthermore, the formulation considers micromechanical models for FRP that also makes it possible to take into account the fiber orientation relative to the sliding direction, the fiber volume fraction, the aspect ratio of fibers, or the fiber arrangement. The proposed contact and wear laws, as well as the numerical methodology, are applied to compute and study wear in a carbon FRP. In these studies, it can be observed how the fiber orientation, micromechanics, or sliding orientation affect the normal and tangential contact compliance, as well as the contact traction distribution and wear evolution.

Keywords: Unidirectional Composites, Fretting Wear, Anisotropic Friction, Contact Mechanics, Micromechanics, Boundary Element Method.

1. Introduction

Fiber-reinforced composite materials are increasingly being applied in many different structural and mechanical components in Aerospace, Automobile, Biomedicine [Scholz, Blanchfield, Bloom, Coburn, Elkington, Fuller, Gilbert, Muflahi, Pernice, Rae, Trevarthen, White, Weaver, and Bond (2011)] or Building and Civil applications [Bank (2006)], due to their high values of specific strength and stiffness, biocompatibility or durability. In many of these structural components, fiber-reinforced plastics (FRP) are subjected to contact and interface loads. Some

[1] Escuela Técnica Superior de Ingenieros, Universidad de Sevilla, Camino de los Descubrimientos s/n , Sevilla E-41092, Spain. E-mail: luisroteso@us.es

[2] Department of Aeronautics, Imperial College London, South Kensington Campus, London SW7 2AZ, UK. E-mail: m.h.aliabadi@imperial.ac.uk

examples can be observed in mechanical joints between FRP profiles and stainless steel connections, or pin-loaded FRP plates.

Although FRP are widely applied in many structural and mechanical systems, there are not many numerical formulations that allow to analyze these polymer composites under different contact and wear conditions, especially due to the fact that particular contact and wear constitutive laws are required. Some experimental works have studied the significant influence of fiber orientation on the wear and frictional behavior of FRP composites. The works of [Ohmae, Kobayashi, and Tsukizoe (1974); Sung and Suh (1979); Tsukizoe and Ohmae (1983); Cirino, Friedrich, and Pipes (1988); Jacobs, Friedrich, Marom, Schulte, and Wagner (1990); Vishwanath, Verma, and Rao (1993)] and the book of [Friedrich (1993)], and more recently, the works of [Larsen, Andersen, Thorning, Horsewell, and Vigild (2007)] and [Sharma, Rao, and Bijwe (2009)], must be mentioned. Those experimental works showed that the friction coefficient depends on several factors including the combination of materials, the surface roughness or the fiber orientation (i.e. the largest coefficient of friction was obtained when the sliding was normal to the fiber orientation, while the lowest one was obtained when the fiber orientation was transverse) (see Fig.1). Even considering a sliding direction on a plane parallel to the direction of fibers, [Ohmae, Kobayashi, and Tsukizoe (1974)] observed that the friction coefficient sliding in parallel direction was smaller than in the transverse direction. So proper contact constitutive laws have to take into account the fiber orientation. Furthermore, experimental works also show the importance of the micromechanics of the anisotropic bulk.

Several semi analytical works have dealt with the problem of FRP contact and interaction modeling. The works of [Ning and Lovell (2002); Ning, Lovell, and Morrow (2004); Ning, Lovell, and Slaughter (2006); Batra and Jiang (2008); Jiang and Batra (2010); Leroux and Nélias (2011); Bagault, Nélias, and Baietto (2012); Bagault, Nélias, Baietto, and Ovaert (2013a)] and [Bagault, Nélias, Baietto, and Ovaert (2013b)] should also be mentioned. However, due to their intrinsic mathematical complexity, analytical solutions incorporate several restrictive assumptions, e.g. rigid indenter, half-plane space, etc.

In the numerical context and based on the Finite Element Method (FEM), the works of [Xiaoyu (1995)] and [Lovell (1998)] started to study some contact problem between composites. The indentation problem of fiber reinforced polymer was initially studied by [Vàradi, K., Flöck, and Friedrich (1998)]. Later, [Vàradi, Nèder, Friedrich, and Flöck (1999)] presented a FEM formulation involving macro- and micro-contact analysis, and more recently, [Goda, Vàradi, Wetzel, and Friedrich (2004a,b)] studied the fiber–matrix debonding process. As it can be observed in these works, a very fine mesh must be considered to approximate the contact

problem between these composite domains. The Boundary Element Method (BEM) has been a well recognized, in general, very accurate and efficient numerical tool for studying contact and interface problems in FRP materials. Using the BEM, [Okada, Fukui, and Kumazawa (2004)] and [Wang and Yao (2005)] studied particle-reinforced composites, [Araújo and Gray (2008)] and [Wang and Z.H.Yao (2008)] simulated carbon nanotube reinforced composites and [Távara, Mantic, Graciani, Canas, and París (2010)] analyzed composite interlaminar crack propagation. [Varna, Paris, and del Cano (1997); Han, Ingber, and Schreyer (2006); Graciani, Mantic, París, and Varna (2009)] and [Távara, Mantic, Graciani, and París (2011)] studied the fiber–matrix debonding problem, [Mallardo and Alessandri (2000)] deal with optimization/identification analysis of inclusions (i.e. fibers) in frictionless unilateral contact with the matrix, and [Rodríguez-Tembleque, Buroni, Abascal, and Sáez (2013)] and [Rodríguez-Tembleque, Sáez, and Buroni (2013)] studied fiber reinforced composites under frictional indentation problems. However, all these numerical works solve different contact problems assuming frictionless contact, or constant friction (and wear) coefficients, which are, for example, independent of fiber orientation and sliding direction.

This work presents new contact constitutive laws for friction and wear modelling in FRP. These proposed laws are incorporated to a boundary-element-based methodology like [Rodríguez-Tembleque, Abascal, and Aliabadi (2010, 2011); Rodríguez-Tembleque, Buroni, Abascal, and Sáez (2011); Rodríguez-Tembleque, Abascal, and Aliabadi (2012a,b); Rodríguez-Tembleque and Abascal (2013)], which allows to solve the contact problem taking into account both the mechanical and the tribological anisotropic characteristics (i.e. anisotropic bulk properties and anisotropic wear and frictional conditions). Furthermore, the formulation considers micromechanical models for FRP [Hopkins and Chamis (1988)] and [TuckerIII and Liang (1999)], that also makes it possible to consider the fiber orientation relative to the sliding direction, the fiber volume fraction, the aspect ratio of fibers, or the fiber arrangement. The proposed contact and wear laws, and the numerical methodology, are applied to compute and study wear in carbon FRP, showing the influence of fiber volume fraction, fiber orientation and sliding orientation and fiber aspect ratio on contact tractions, normal and tangential contact compliance or wear evolution.

2. Contact problem formulation

The contact problem between two linear anisotropic elastic bodies Ω^α, $\alpha = 1,2$ with boundary $\partial\Omega^\alpha$ defined in the Cartesian coordinate system $\{x_i\}$ in $\mathbb{R}^3$ is considered. In order to know the relative position between both bodies at all times (τ), a gap variable is defined for the pair $I \equiv \{P^1, P^2\}$ of points ($P^\alpha \in \partial\Omega^\alpha, \alpha = 1,2$),

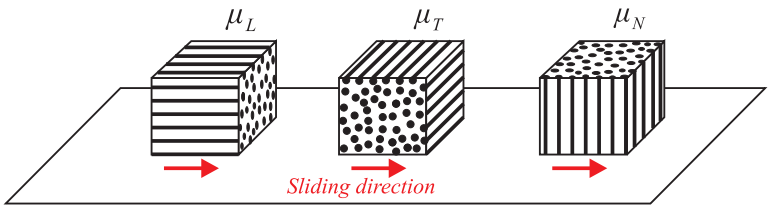

(a) (b) (c)

Figura 1: Schematic diagram of a unidirectional FRP indicating the sliding directions: (a) Longitudinal, (b) Transverse, and (c) Normal ($\mu_L \leq \mu_T \leq \mu_N$).

as $\mathbf{g} = \mathbf{B}^T(\mathbf{x}^2 - \mathbf{x}^1)$, where $\mathbf{x}^\alpha$ is the position of P^α at every instant ($\mathbf{x}^\alpha = \mathbf{X}^\alpha + \mathbf{u}_o^\alpha + \mathbf{u}^\alpha$), and matrix $\mathbf{B} = [\mathbf{e}_1|\mathbf{e}_2|\mathbf{n}]$ is a base change matrix defined in [Rodríguez-Tembleque, Abascal, and Aliabadi (2012a,b); Rodríguez-Tembleque and Abascal (2013); Rodríguez-Tembleque, Buroni, Abascal, and Sáez (2013)] and [Rodríguez-Tembleque, Sáez, and Buroni (2013)], which expresses the pair I gap in relation to the local orthonormal base (see Fig. 2).

The expression for the gap can be written as:

$$\mathbf{g} = \mathbf{g}_{go} + \mathbf{B}^T(\mathbf{u}^2 - \mathbf{u}^1) \tag{1}$$

where $\mathbf{g}_{go} = \mathbf{g}_g + \mathbf{g}_o$, $\mathbf{g}_g = \mathbf{B}^T(\mathbf{X}^2 - \mathbf{X}^1)$ is the *geometric gap* between two solids in the reference configuration, and $\mathbf{g}_o = \mathbf{B}^T(\mathbf{u}_o^2 - \mathbf{u}_o^1)$ the gap due to the *rigid body movements*. In this work, the reference configuration for each solid ($\mathbf{X}^\alpha$) that will be considered is the initial configuration (before applying load). Consequently, $\mathbf{g}_g$ may also be termed *initial geometric gap*. In Eq.(1) two components can be identified: the normal gap, $g_n = g_{go,n} + u_n^2 - u_n^1$, and the tangential gap or *slip*, $\mathbf{g}_t = \mathbf{g}_{go,t} + \mathbf{u}_t^2 - \mathbf{u}_t^1$, being u_n^α and $\mathbf{u}_t^\alpha = [u_{t1}^\alpha, u_{t2}^\alpha]$ the normal and tangential components of the displacements.

3. Anisotropic frictional contact law

The unilateral contact law involves two conditions in the *Contact Zone* (Γ_c): impenetrability and no cohesion. Therefore for each pair $I \equiv \{P^1, P^2\} \in \Gamma_c$: $g_n \geq 0$ and $t_n \leq 0$. The variable t_n is the normal contact traction defined as: $t_n = \mathbf{B}_n^T\mathbf{t}^1 = -\mathbf{B}_n^T\mathbf{t}^2$, where $\mathbf{t}^\alpha$ is the traction of point $P^\alpha \in \Gamma_c^\alpha$ expressed in the global system of reference, and $\mathbf{B}_n = [\mathbf{n}]$ is the third column of matrix $\mathbf{B} = [\mathbf{B}_t|\mathbf{B}_n]$. Tangential traction is defined as: $\mathbf{t}_t = \mathbf{B}_t^T\mathbf{t}^1 = -\mathbf{B}_t^T\mathbf{t}^2$. Finally, the variables g_n and t_n are complementary:

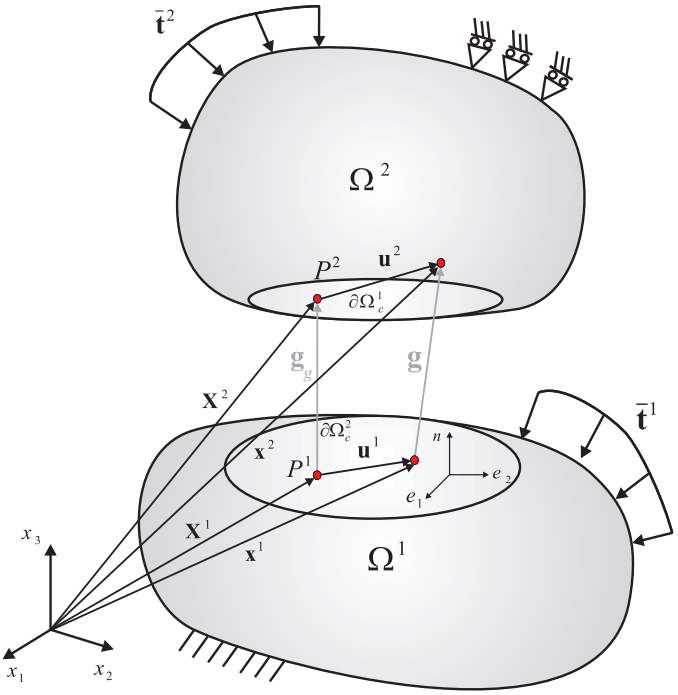

Figura 2: Contact pair I of points $P^\alpha \in \partial\Omega^\alpha$ ($\alpha = 1,2$).

$g_n\ t_n = 0$, so this set of relations may be summarized as the so-called Signorini conditions: $g_n \geq 0$, $t_n \leq 0$, $g_n\ t_n = 0$.

Friction constitutive laws for FRP can be accurately approximated by a convex elliptical friction cone, according to experimental works. The principal axes of the ellipse coincide with the orthotropic axes (Fig.3(a)). The generic form of such anisotropic limit friction is given by

$$f(\mathbf{t}_t, t_n) = ||\mathbf{t}_t||_\mu - |t_n| = 0 \tag{2}$$

where $||\bullet||_\mu$ denotes the elliptic norm $||\mathbf{t}_t||_\mu = \sqrt{(t_{e_1}/\mu_1)^2 + (t_{e_2}/\mu_2)^2}$, and the coefficients μ_1 and μ_2 are the principal friction coefficients in the directions $\{e_1, e_2\}$. Eq. (2) constitutes an ellipse whose principal axes are: $\mu_1|t_n|$ and $\mu_2|t_n|$ (see Fig. 3(b)). The classical isotropic Coulomb's friction criterion is recovered in Eq.(2) considering $\mu_1 = \mu_2 = \mu$. The allowable contact tractions $\mathbf{t}$ must satisfy: $f(\mathbf{t}_t, t_n) \leq 0$, defining an admissible convex region for $\mathbf{t}$: the *Friction Cone* ($\mathbb{C}_f$). An as-

sociated sliding rule is considered, so the sliding direction is given by the gradient to the friction cone and its magnitude by the factor λ: $\dot{g}_{e_1} = -\lambda \partial f/\partial t_{e_1}$ and $\dot{g}_{e_2} = -\lambda \partial f/\partial t_{e_2}$. To satisfy the complementarity relations: $f(\mathbf{t}_t, t_n) \leq 0$, $\lambda \geq 0$, $\lambda f(\mathbf{t}_t, t_n) = 0$, the expression for λ factor is: $\lambda = ||\dot{\mathbf{g}}_t||^*_\mu$, where the norm $||\bullet||^*_\mu$ is dual of $||\bullet||_\mu$, so: $||\dot{\mathbf{g}}_t||^*_\mu = \sqrt{(\mu_1 \dot{g}_{e_1})^2 + (\mu_2 \dot{g}_{e_2})^2}$. Thus: $t_{e_1} = -||\mathbf{t}_t||_\mu \mu_1^2 \dot{g}_{e_1}/||\dot{\mathbf{g}}_t||^*_\mu$ and $t_{e_2} = -||\mathbf{t}_t||_\mu \mu_2^2 \dot{g}_{e_2}/||\dot{\mathbf{g}}_t||^*_\mu$. To sum up, the *unilateral contact condition* and the *elliptic friction law* defined for any pair $I \equiv \{P^1, P^2\} \in \Gamma_c$ of points in contact can be compiled as follows, according to their contact status: *no contact* ($t_n = 0$, $g_n \geq 0$ and $\mathbf{t}_t = \mathbf{0}$), *contact-adhesion* ($t_n \leq 0$, $g_n = 0$ and $\dot{\mathbf{g}}_t = \mathbf{0}$) and *contact-slip* ($t_n \leq 0$, $g_n = 0$ and $\mathbf{t}_t = -|t_n| \mathbb{M}^2 \dot{\mathbf{g}}_t/||\dot{\mathbf{g}}_t||^*_\mu$). The tangential slip velocity ($\dot{\mathbf{g}}_t$) is expressed at time τ_k as: $\dot{\mathbf{g}}_t \simeq \Delta \mathbf{g}_t/\Delta\tau$, where $\Delta \mathbf{g}_t = \mathbf{g}_t(\tau_k) - \mathbf{g}_t(\tau_{k-1})$ and $\Delta\tau = \tau_k - \tau_{k-1}$, according to a standard backward Euler scheme. $\mathbb{M}$ is a diagonal matrix:

$$\mathbb{M} = \begin{bmatrix} \mu_1 & 0 \\ 0 & \mu_2 \end{bmatrix} \tag{3}$$

whose coefficients are

$$\mu_1 = \mu_L + (\mu_N - \mu_L)\ \hat{\varphi} \tag{4}$$

$$\mu_2 = \mu_T + (\mu_N - \mu_T)\ \hat{\varphi} \tag{5}$$

The expressions above establish a new constitutive friction law which can be applied to model friction in FRP. Parameter ($0 \leq \hat{\varphi} \leq 1$) is the nondimensional fiber orientation constant ($\hat{\varphi} = 2\varphi/\pi$), being ($0 \leq \varphi \leq \pi/2$) the fiber orientation relative to direction $\mathbf{e}_1$ (see Fig. 3(c)), and $\{\mu_L, \mu_T, \mu_N\}$ are the friction coefficients in longitudinal, transverse and normal direction, respectively, that can be obtained from experimental works like [Ohmae, Kobayashi, and Tsukizoe (1974)] and [Tsukizoe and Ohmae (1983)]. So the anisotropic friction surface (2) is also a function of the fiber orientation parameter ($\hat{\varphi}$):

$$f(\mathbf{t}_t, t_n, \hat{\varphi}) = ||\mathbf{t}_t||_{\mu(\hat{\varphi})} - |t_n| = 0 \tag{6}$$

In Fig.4 it can be observed how an orthotropic friction cone is obtained when the fibers are parallel to the sliding plane ($\hat{\varphi} = 0$), and an isotropic friction cone is obtained when the fibers are normal to the sliding plane ($\hat{\varphi} = 1$), which it is according to experimental works like [Ohmae, Kobayashi, and Tsukizoe (1974)] and [Sung and Suh (1979)].

The combined normal-tangential contact problem constraints (i.e. the *unilateral contact condition* and the *elliptic friction law*) can be formulated as [Rodríguez-

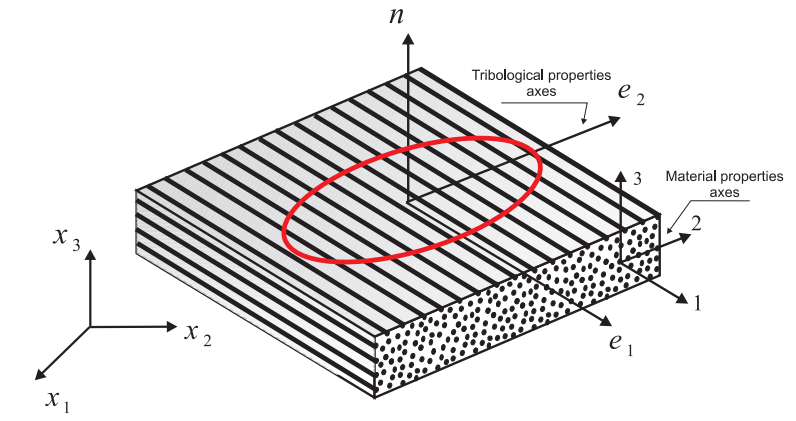

(a)

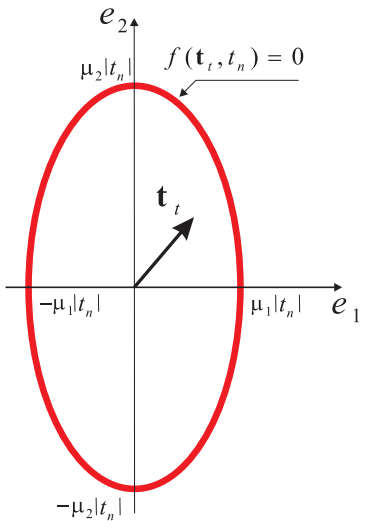

(b)

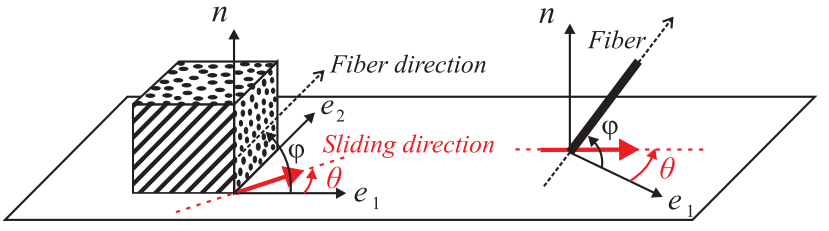

(c)

Figura 3: (a) Continuous parallel fibers perpendicular to normal vector. (b) Elliptic friction law. (c) Unidirectional FRP direction and sliding direction.

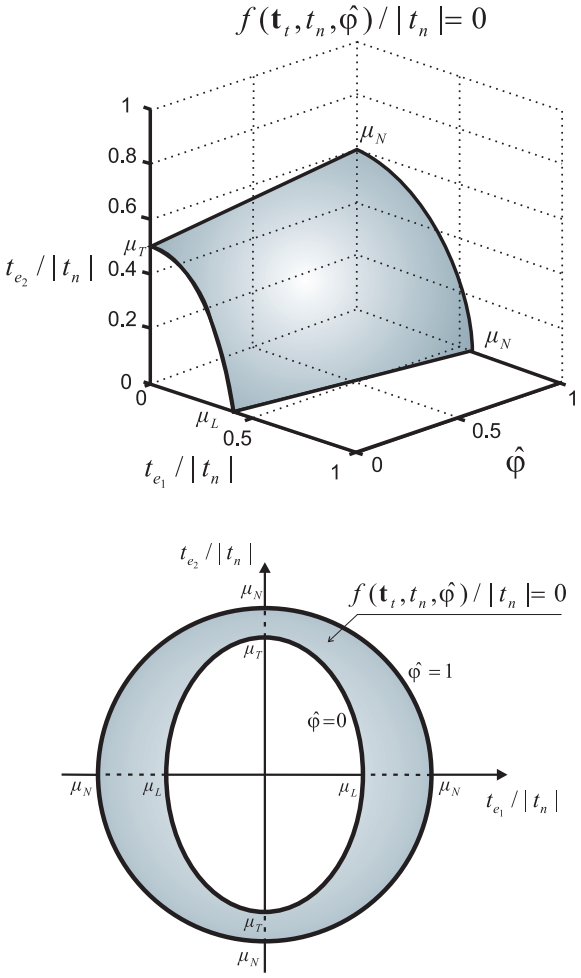

Figura 4: Friction surface ($f(\mathbf{t}_t, t_n, \hat{\boldsymbol{\varphi}})/|t_n| = 0$) as a function of the fiber orientation $\hat{\boldsymbol{\varphi}}$.

Tembleque, Abascal, and Aliabadi (2012a,b)] and [Rodríguez-Tembleque and Abascal (2013)]:

$$\mathbf{t} - \mathbb{P}_{\mathbb{C}_f}(\mathbf{t}^*) = \mathbf{0} \tag{7}$$

where the contact operator $\mathbb{P}_{\mathbb{C}_f}$ was defined as $\mathbb{P}_{\mathbb{C}_f}(\mathbf{t}^*) = \{ \ \mathbb{P}_{\mathbb{E}_\rho}(\mathbf{t}_t^*) \quad \mathbb{P}_{\mathbb{R}_-}(t_n^*) \ \}^T$. The normal projection function, $\mathbb{P}_{\mathbb{R}_-}(\cdot)$, and the tangential projection function, $\mathbb{P}_{\mathbb{E}_\rho}$

were also defined in [Rodríguez-Tembleque, Abascal, and Aliabadi (2012a,b)] and [Rodríguez-Tembleque and Abascal (2013)], as well as the augmented traction components $(\mathbf{t}^*)^T = [(\mathbf{t}_t^*)^T t_n^*]$: $\mathbf{t}_t^* = \mathbf{t}_t - r_t \mathbb{M}^2 \mathbf{g}_t$ and $t_n^* = t_n + r_n g_n$. The parameters r_n and r_t are the normal and tangential dimensional penalization parameters ($r_n \in \mathbb{R}^+, r_t \in \mathbb{R}^+$), respectively.

4. Anisotropic wear law

A quasi-steady-state wear approximation similar to [Rodríguez-Tembleque, Abascal, and Aliabadi (2010, 2011, 2012a,b)], [Paczelt, Kucharski, and Mróz (2012)], [Paczelt and Mróz (2012)], [Stupkiewicz (2013)], [Cavalieri and Cardona (2013)] and [Lengiewicz and Stupkiewicz (2013)], is considered. The wear constitutive law is based on [Rodríguez-Tembleque, Abascal, and Aliabadi (2012a,b)]. In this work, wear evolution can be expressed in the following wear rate form: $\dot{g}_w = i_w \, |t_n| \dot{D}_s$, g_w being the wear depth, $\dot{D}_s$ the tangential slip velocity module ($\dot{D}_s = ||\dot{\mathbf{g}}_t||$), and i_w, the dimensional wear coefficient or the specific wear rate. Assuming that the wear intensity i_w is a function of the sliding direction parameter α_v ($i_w = i_w(\alpha_v)$), wear velocity ($\dot{g}_w$) depends on the sliding direction. α_v is the measure of the oriented angle between the given direction ($\mathbf{e}_1$) and the sliding velocity direction. Let us consider an orthotropic wear law, $i_w(\alpha_v) = \sqrt{(i_1 \cos\alpha_v)^2 + (i_2 \sin\alpha_v)^2}$, where: $\cos\alpha_v = \dot{g}_{e_1}/||\dot{\mathbf{g}}_t||$, $\sin\alpha_v = \dot{g}_{e_2}/||\dot{\mathbf{g}}_t||$, and i_1 and i_2 are the principal intensity coefficients:

$$i_1 = i_L + (i_N - i_L)\ \hat{\varphi} \tag{8}$$

$$i_2 = i_T + (i_N - i_T)\ \hat{\varphi} \tag{9}$$

whose expressions (8) and (9) establish a new constitutive wear law which can be applied to model friction in FRP. Finally, postulating the wear rate to be proportional to the friction dissipation energy makes $i_L = k\mu_L|t_n|$, $i_T = k\mu_T|t_n|$ and $i_N = k\mu_N|t_n|$, so they are related to friction coefficients through the wear factor k. So the wear intensity can be written as $i_w = ||\dot{\mathbf{g}}_t||_i / ||\dot{\mathbf{g}}_t||$, being $||\dot{\mathbf{g}}_t||_i = \sqrt{(i_1 \dot{g}_{e_1})^2 + (i_2 \dot{g}_{e_2})^2}$. Finally, the anisotropic wear law can be defined by

$$\dot{g}_w = |t_n| \ ||\dot{\mathbf{g}}_t||_i \tag{10}$$

For quasi-static contact problems, wear depth defined on instant τ_k, is computed as

$$g_w = g_w(\tau_{k-1}) + |t_n| \ ||\Delta\mathbf{g}_t||_i \tag{11}$$

$g_w(\tau_{k-1})$ being the wear depth value on instant τ_{k-1}. Due to the fact that the depth of removed material is computed for an instant τ_k, the normal contact gap (g_n) at the same time must be rewritten: $g_n = g_{go,n} + (u_n^2 - u_n^1) + g_w$.

5. Contact discrete variables and restrictions

The contact tractions ($\mathbf{t}_c$), the gap ($\mathbf{g}$), and the displacements ($\mathbf{u}^\alpha$, $\alpha = 1,2$), are discretized over the contact interface (Γ_c). To that end, Γ_c is divided into N^f elemental surfaces (Γ_c^e). These elements (Γ_c^e) constitute a *contact frame*. The contact tractions are discretized over the contact frame as: $\mathbf{t}_c \simeq \hat{\mathbf{t}}_c = \sum_{i=1}^{N^f} \delta_{P_i} \lambda_i$, where δ_{P_i} is the Dirac delta on each contact frame node i, and λ_i is the Lagrange multiplier on the node ($i = 1...N^f$) and collected in vector Λ. In the same way, the gap is approximated as $\mathbf{g} \simeq \hat{\mathbf{g}} = \sum_{i=1}^{N^f} \delta_{P_i} \mathbf{k}_i$. In the expression above, $\mathbf{k}_i$ is the nodal value. Therefore, taking into account the gap approximation, the discrete expression of Eq. 1 can be written as:

$$(\mathbf{k})_I = (\mathbf{k}_{go})_I + (\mathbf{d}^2)_I - (\mathbf{d}^1)_I \tag{12}$$

for every contact pair I. In the expression above, $\mathbf{k}$ is the contact pairs gap vector and $\mathbf{k}_{go}$ the initial geometrical gap and translation vector. Finally, the contact restrictions (Eq. (7)) for every contact pair I can be expressed as:

$$(\Lambda_t)_I - \mathbb{P}_{\mathbb{E}_\rho}(\,(\Lambda_t^*)_I) = \mathbf{0} \tag{13}$$

$$(\Lambda_n)_I - \mathbb{P}_{\mathbb{R}_-}(\,(\Lambda_n^*)_I) = 0 \tag{14}$$

where augmented contact variables are defined as: $(\Lambda_t^*)_I = (\Lambda_t)_I - r_t \mathbb{M}^2(\mathbf{k}_t)_I$ and $(\Lambda_n^*)_I = (\Lambda_n)_I + r_n(\mathbf{k}_n)_I$, and the value of ρ for the I pair: $\rho = |\mathbb{P}_{\mathbb{R}_-}(\,(\Lambda_n^*)_I)|$.

6. Discrete boundary element coupling equations for solids

The BEM formulation for an elastic continuum Ω with boundary $\partial\Omega$ is well known and can be found in many classical texts such as [Aliabadi (2002)]. For a boundary point ($P \in \partial\Omega$), the *Somigliana identity* can be written as:

$$\tilde{\mathbf{C}}\,\mathbf{u}(P) + CPV\left\{\int_{\partial\Omega} \mathbf{T}^*\mathbf{u}\; dS\right\} = \int_\Omega \mathbf{U}^*\mathbf{b}\; d\Omega + \int_{\partial\Omega} \mathbf{U}^*\mathbf{t}\; dS \tag{15}$$

where $\mathbf{u}$, $\mathbf{t}$ and $\mathbf{b}$ are, respectively, the displacements, the boundary tractions and the body forces of Ω. $\mathbf{U}^* = \{U_{ij}^*(P,Q)\}$ is the fundamental solution tensor for displacement (free-space Green's functions), and $\mathbf{T}^* = \{T_{ij}^*(P,Q)\}$ stands for the tractions fundamental solution at point Q in the ith direction due to a unit load applied at point P in the jth direction. The matrix $\tilde{\mathbf{C}}$ is equal to $\frac{1}{2}\,\mathbf{I}$ for a smooth boundary $\partial\Omega$, and $CPV\,\{\int \cdot\, dS\}$ denotes the *Cauchy Principal Value* of the integral $\int \cdot\, dS$.

The integral Equation (15) can be written as follows:

$$\tilde{\mathbf{C}}\mathbf{u}(P) + \sum_{e=1}^{N_e} \left\{ \int_{\partial\Omega^e} \mathbf{T}^* \mathbf{u} \, dS \right\} = \sum_{e=1}^{N_e} \left\{ \int_{\partial\Omega^e} \mathbf{U}^* \mathbf{t} \, dS \right\} \tag{16}$$

in case of absence of body loads ($\mathbf{b} = \mathbf{0}$), where the boundary $\partial\Omega$ is divided into N_e elements, $\partial\Omega^e \in \partial\Omega$, so: $\partial\Omega = \bigcup_{e=1}^{N_e} \partial\Omega^e$ and $\bigcap_{e=1}^{N_e} \partial\Omega^e = \emptyset$. The fields $\mathbf{u}$ and $\mathbf{t}$ are approximated over each element $\partial\Omega^e$ using shape functions, as a function of the nodal values ($\mathbf{d}^e$ and $\mathbf{p}^e$): $\mathbf{u} \simeq \hat{\mathbf{u}} = \mathbf{N}\mathbf{d}^e$ and $\mathbf{t} \simeq \hat{\mathbf{t}} = \mathbf{N}\mathbf{p}^e$, being $\mathbf{N}$ the shape functions approximation matrix.

In this work, the fundamental solution considered for an anisotropic media is the one recently presented by [Buroni and Sáez (2013)], so after the discretization, the Eq.(16) can be written as

$$\tilde{\mathbf{C}}_i \mathbf{u}_i + \sum_{j=1}^{N} \tilde{\mathbf{H}}_i^e \mathbf{d}^e = \sum_{j=1}^{N} \tilde{\mathbf{G}}_i^e \mathbf{p}^e \tag{17}$$

being: $\tilde{\mathbf{H}}_i^e = \int_{\partial\Omega^e} \mathbf{T}^* \mathbf{N} \, d\Gamma$, $\tilde{\mathbf{G}}_i^e = \int_{\partial\Omega^e} \mathbf{U}^* \mathbf{N} \, d\Gamma$, the integrals over the element e when the collocation point is the node i. Finally, the contribution for all i nodes can be written together in matrix form to give the global system of equations,

$$\tilde{\mathbf{H}}\mathbf{d} - \tilde{\mathbf{G}}\mathbf{p} = \mathbf{F} \tag{18}$$

where $\mathbf{d}$ and $\mathbf{p}$ are the displacements and tractions nodal vectors, respectively. Matrices $\tilde{\mathbf{G}}$ and $\tilde{\mathbf{H}}$ are constructed collecting the terms of matrices $\tilde{\mathbf{H}}_i^e$ and $\tilde{\mathbf{G}}_i^e$, and $\mathbf{F}$ contains the applied boundary conditions.

Eq.(18) can be written for contact problems as: $\mathbf{A}_\mathrm{x}\mathbf{x} + \mathbf{A}_p\mathbf{p}_c = \mathbf{F}$, being $(\mathbf{x})^T = [(\mathbf{x}_e)^T \ (\mathbf{d}_c)^T]$ the nodal unknowns vector that collects the external unknowns ($\mathbf{x}_e$), and the contact nodal displacements ($\mathbf{d}_c$). $\mathbf{p}_c$ is the nodal contact tractions. $\mathbf{A}_p$ is constructed with the columns of $\tilde{\mathbf{G}}$ belonging to the contact nodal unknowns, and $\mathbf{A}_\mathrm{x} = [\mathbf{A}_\mathrm{x} \ \mathbf{A}_d]$ with the columns matrices $\tilde{\mathbf{H}}$ and $\tilde{\mathbf{G}}$, corresponding to the exterior unknowns ($\mathbf{A}_\mathrm{x}$), and the contact nodal displacements ($\mathbf{A}_d$).

Considering a boundary element discretization for every solid Ω^α ($\alpha = 1, 2$), the resulting BEM-BEM non-linear coupling equations set can be expressed according to [Rodríguez-Tembleque, Abascal, and Aliabadi (2012b)], as

$$\begin{bmatrix} \mathbf{A}_\mathrm{x}^1 & \mathbf{0} & \mathbf{A}_p^1 \tilde{\mathbf{C}}^1 & \mathbf{0} \\ \mathbf{0} & \mathbf{A}_\mathrm{x}^2 & -\mathbf{A}_p^2 \tilde{\mathbf{C}}^2 & \mathbf{0} \\ (\mathbf{C}^1)^T & -(\mathbf{C}^2)^T & \mathbf{0} & \mathbf{C}_g \end{bmatrix} \begin{Bmatrix} \mathbf{x}^1 \\ \mathbf{x}^2 \\ \Lambda \\ \mathbf{k} \end{Bmatrix} = \begin{Bmatrix} \mathbf{F}^1 \\ \mathbf{F}^2 \\ \mathbf{C}_g \mathbf{k}_{go} \end{Bmatrix} \tag{19}$$

The first two groups of rows in the expression above represent the equilibrium of each solid Ω^α ($\alpha = 1,2$). The third row is the contact kinematics equations and the last row express the nodal contact restrictions. Vector Λ represents the nodal contact tractions, so that: $\mathbf{p}_c^1 = \tilde{\mathbf{C}}^1\Lambda$ and $\mathbf{p}_c^2 = -\tilde{\mathbf{C}}^2\Lambda$. Eq.(19) can be expressed, according to Rodríguez-Tembleque, Abascal, and Aliabadi (2012b), as:

$$\begin{bmatrix} \mathbf{R}^1 & \mathbf{R}^2 & \mathbf{R}_\lambda & \mathbf{R}_g \end{bmatrix} \begin{Bmatrix} \mathbf{x}^1 \\ \mathbf{x}^2 \\ \Lambda \\ \mathbf{k} \end{Bmatrix} = \bar{\mathbf{F}} \tag{20}$$

$\mathbf{x}^\alpha$ being the solid Ω^α ($\alpha = 1,2$) unknowns, vector Λ represents the nodal contact tractions, and the matrices $\mathbf{R}^1$, $\mathbf{R}^2$, $\mathbf{R}_\lambda$ and $\mathbf{R}_g$, and vector $\bar{\mathbf{F}}$, the corresponding block matrices of these coupling systems.

7. Wear equations for contact problems

The wear depth for every instant can be discretized over the contact frame, as a function of the nodal values as $g_w^{(k)} \simeq \hat{g}_w^{(k)} = \tilde{\mathbf{N}}\mathbf{w}^e$, being $\tilde{\mathbf{N}}$ the shape functions matrix defined for the frame element Γ_c^e, and $\mathbf{w}^e$ the nodal wear depth vector of element Γ_c^e. Therefore, the discrete form of kinematic equation for I pair, at instant k, is

$$(\mathbf{k}^{(k)})_I = (\mathbf{k}_{go}^{(k)})_I + (\mathbf{d}^{2\,(k)})_I - (\mathbf{d}^{1\,(k)})_I + (\mathbf{C}_{g_n}\mathbf{w}^{(k)})_I \tag{21}$$

where $\mathbf{w}^{(k)}$ is a vector which contains the contact pairs wear depth, and matrix $\mathbf{C}_{g_n}$ is constituted using the $\mathbf{C}_g$ columns which affect the normal gap of contact pairs [Rodríguez-Tembleque, Abascal, and Aliabadi (2012a,b)]. The discrete expression of Eq. (11) can be written for I pair as

$$(\mathbf{w}^{(k)})_I = (\mathbf{w}^{(k-1)})_I + |(\Lambda_n^{(k)})_I|\ ||(\mathbf{k}_t^k)_I - (\mathbf{k}_t^{(k-1)})_I||_i \tag{22}$$

where $\Lambda_n^{(k)}$ is a vector which contains the normal traction components of contact pairs at instant k.

8. Solution Scheme

The quasi-static wear contact problem equations set Eq.$\{$(13), (14), (20-22)$\}$ allow to compute the variables on instant or load step (k), $\mathbf{z}^{(k)} = [(\mathbf{x}^1)^T\ (\mathbf{x}^2)^T\ \Lambda^T\ \mathbf{k}^T\ \mathbf{w}^T]^T$, when the variables on previous instant are known. In this work $\mathbf{z}^{(k)}$ is computed using the iterative Uzawa predictor-corrector scheme proposed in [Rodríguez-Tembleque, Abascal, and Aliabadi (2012a,b)] and [Rodríguez-Tembleque and Abascal (2013)]:

(I) Initialization: $\mathbf{z}^{(0)} = \mathbf{z}^{(k-1)}$.

(II) Predictor step, solve:

$$\left[\begin{array}{ccc} \mathbf{R}^1 & \mathbf{R}^2 & \mathbf{R}_g \end{array} \right] \left[\begin{array}{c} \mathbf{x}^1 \\ \mathbf{x}^2 \\ \mathbf{k} \end{array} \right]^{(n+1)} = -\mathbf{R}_\lambda \, \Lambda^{(n)} + \bar{\mathbf{F}}^{(k)} \tag{23}$$

being

$$\bar{\mathbf{F}}^{(k)} = \left[\begin{array}{c} \mathbf{F}^{1(k)} \\ \mathbf{F}^{2(k)} \\ \mathbf{C}_g \left(\mathbf{k}_g + \mathbf{k}_o^{(k-1)} + \Delta \mathbf{k}_o^{(n)} + \mathbf{C}_{g_n} \mathbf{w}^{(k-1)} \right) \end{array} \right] \tag{24}$$

In the expressions above, k is the load step index, whereas n is the iteration index inside the load step.

(III) Corrector step, update the contact tractions $\Lambda^{(n+1)}$ for every contact pair I:

$$(\Lambda_n^{(n+1)})_I = \mathbb{P}_{\mathbb{R}_-}(\, (\Lambda_n^{(n)})_I + r_n (\mathbf{k}_n^{(n+1)})_I \,) \tag{25}$$

$$(\Lambda_t^{(n+1)})_I = \mathbb{P}_{\mathbb{E}_\rho}(\, (\Lambda_t^{(n)})_I - r_t \, \mathbb{M}^2 (\Delta \mathbf{k}_t^{(n+1)})_I \,) \tag{26}$$

being $(\Delta \mathbf{k}_t^{(n+1)})_I = [(\mathbf{k}_t^{(n+1)})_I - (\mathbf{k}_t^{(k-1)})_I]$, $\rho = |(\Lambda_n^{(n+1)})_I|$, and the resulting accumulated wear depth:

$$(\mathbf{w}^{(n+1)} \,)_I = (\mathbf{w}^{(k-1)} \,)_I + |(\, \Lambda_n^{(n+1)} \,)_I| \; || \; (\Delta \mathbf{k}_t^{(n+1)})_I \; ||_i \tag{27}$$

(IV) Compute the error function: $\Psi(\Lambda^{(n+1)}) = \|\Lambda^{(n+1)} - \Lambda^{(n)}\|$.

(a) If $\Psi(\Lambda^{(n+1)}) \leq \varepsilon$, the solution for the instant (k) is reached: $\mathbf{z}^{(k)} = \mathbf{z}^{(n+1)}$. Only in case the applied boundary condition is the external load j-component ($\mathbf{Q}_j^{(k)}$), before reaching the solution for instant (k), the resultant applied loads on the contact zone (Γ_c) have to be calculated:

$$\mathbf{Q}_j^{(n+1)} = \int_{\Gamma_c} \Lambda_j^{(n+1)} \, d\Gamma \tag{28}$$

(a.1) If $|\mathbf{Q}_j^{(n+1)}| > |\mathbf{Q}_j^{(k)}| + \varepsilon_{load}$, modify $\Delta\mathbf{k}_o^{(n)}$ and return to (II).

(a.2) Otherwise, the solution for instant (k) is reached: $\mathbf{z}^{(k)} = \mathbf{z}^{(n+1)}$.

(b) Otherwise, return to (II) evaluating: $\Lambda^{(n)} = \Lambda^{(n+1)}$ and iterate until the convergence is reached.

After the solution at instant (k), $\mathbf{z}^{(k)}$, is reached, the solution for the next instant is achieved by setting: $\mathbf{z}^{(k-1)} = \mathbf{z}^{(k)}$ and returning to (I).

9. Numerical studies

A steel sphere of radius $R = 50$ *mm* is indented on a carbon FRP half-space (see Fig. 5(a)). The carbon FRP considered is IM7 Carbon/ $8551-7$, whose mechanical properties of fiber and matrix can be found in [Kaddour and Hinton (2012)] (Table 1). Not only does the fiber orientation have a considerable influence on the contact pressure distribution, the variation of fiber volume fraction or the fiber aspect ratio have to be considered when contact or wear in FRP are computed. Micromechanics allows to estimate the mechanical properties of composite materials from the known values of the fiber and the matrix. There are different micromechanical approaches. The simplest approach is the *rule of mixtures*, but it fails to represent some of the properties with reasonable accuracy. A modified and more accurate micromechanical model was proposed by [Hopkins and Chamis (1988)]. Also Halpin-Tsai proposed semi-empirical equations that have long been applied to predict the properties of short-fiber composites. A detailed review of their derivation is given in [TuckerIII and Liang (1999)]. Both models are considered in the studies, although in the literature, very sophisticated numerical models [Dong and Atluri (2012, 2013)], that take into account micromechanics in heterogeneous materials, can be found.

For simplicity, due to fact that the contact half-width (a) will be much less than the radius (R), the solids are approximated by elastic half-spaces, each one discretized using 320 linear quadrilateral boundary elements. Fig. 5(b) shows the details of the meshes, where the half-space characteristic dimension is $L = 1{,}2$ *mm*.

9.1. Spherical indentation problem: validation

In order to validate the contact formulation, a finite element model has been developed with the commercial FE software ANSYS (version 13.0). The mesh is shown in Fig. 5(c) and it considers 23017 finite elements to discretize the solids: a quarter of sphere and a block of $100 \times 50 \times 50$ *mm*. The sphere is subjected to a normal indentation $g_{o,x_3} = -0{,}02$ *mm* over a IM7 Carbon/ $8551-7$ with a volume fraction of 30 % and fiber alignment: $\varphi = 0^o$. Both FE and BE Hertzian pressure distribution are compared in Fig. 6. An excellent agreement between both solutions can be

Cuadro 1: Mechanical properties of fiber and matrix.

Fiber	IM7
Longitudinal Young modulus E_{f1} (GPa)	276
Transverse Young modulus E_{f2} (GPa)	19
Transverse Young modulus E_{f3} (GPa)	19
In-plane shear modulus G_{f12} (GPa)	27
Transverse shear modulus G_{f23} (GPa)	7
Poisson ratio ν_{f12}	0.2
Poisson ratio ν_{f13}	0.2
Matrix	$8551-7$ epoxy
Elastic modulus E_{m} (GPa)	4.08
Elastic shear modulus G_{m} (GPa)	1.478
Poisson ratio ν_{m}	0.38

observed. Both experiments were conducted on a Windows 7 64-bit machine with the following hardware: Intel Core i5 CPU running at 2.5GHz with 8 GB of memory. As the number of elements are significantly higher in the FE approximation, the BE one is about four times faster than ANSYS for the considered meshes.

9.2. FRP normal and tangential compliance studies

Now, the sphere is subjected to a normal displacement $g_{o,x_3} = -0{,}02$ *mm* and a tangential translational displacement of module: $g_{o,t} = 0{,}008$ *mm*, which forms an angle θ with axis x_1 (see Fig. 5(a)). The proposed frictional law is considered, being the friction coefficients: $\mu_L = 0{,}4$, $\mu_T = 0{,}5$ and $\mu_N = 0{,}55$, according to [Ohmae, Kobayashi, and Tsukizoe (1974)] for carbon FRP. In this indentation problem is studied the influence of: the fiber orientation, the sliding direction, and the micromechanics of FRP (i.e. the fiber volume fraction or the aspect ratio of fibers in the contact variables.

First, the influence of fiber orientation and fiber volume fraction on normal and contact compliance are considered for continuous fiber composites. The influence of fiber volume fraction $\bar{V}_{\mathrm{f}}$ can be studied for: $\bar{V}_{\mathrm{f}} = \{0{,}30, 0{,}45, 0{,}60\}$. Figures 7 (a) and (b) show the normal and tangential contact compliance variation with the fiber orientation and fiber volume fraction, relative to the load for the fiber alignment $\varphi = 0^o$ and $\bar{V}_{\mathrm{f}} = 0{,}30$.

For the normal load (Fig. 7(a)), the largest loads occur in the normal fiber orientation ($\varphi = 90^o$), and high differences can be observed for φ greater than 45^o. The tangential contact compliance relative to the load $Q(\varphi = 0)$ (see Fig. 7(b)), pre-

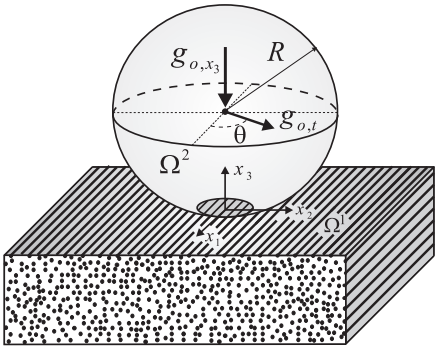

(a)

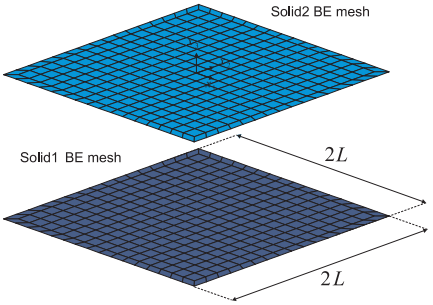

(b)

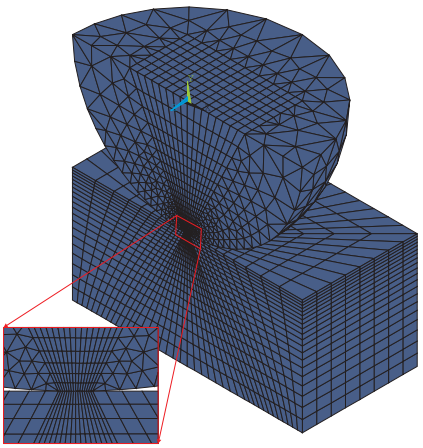

(c)

Figura 5: (a) Sphere indentation over a FRP halfspace. (b) Boundary elements mesh details. (c) Finite elements mesh details.

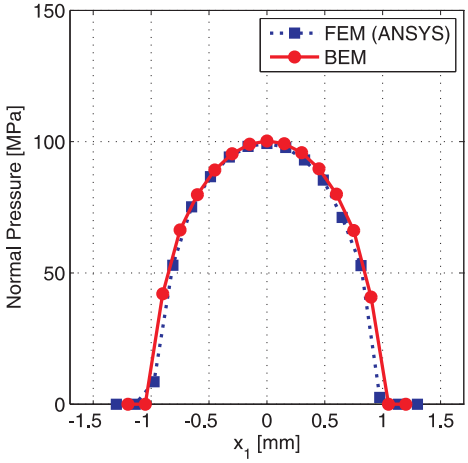

Figura 6: Contact pressure profile for a IM7 Carbon/ 8551 − 7 with a volume fraction of 30 %, considering FE and BE approximations.

sents a different behavior. The largest discrepancies occur for a fiber orientation in the interval $[0^o, 45^o]$. It can be observed in both cases, how normal and tangential contact compliances increase with the volume fraction $\bar{V}_\mathrm{f}$, and this increase in their values is even more significant when the fiber alignment φ is greater than 45^o.

The behavior of the proposed frictional law is validated studying the influence of the sliding direction θ. Examining the Fig.8, where tangential contact compliance variation for $\bar{V}_\mathrm{f} = 0{,}60$ is presented, it is found that the orientation of the fibers has an important effect on frictional response. For different sliding directions ($\theta = \{0^o, 45^o, 90^o\}$), important discrepancies occur for a fiber orientation in the interval $[0^o, 45^o]$, but for $\varphi = 90^o$, the tangential compliance is not affected by θ. This is because we recover the isotropic frictional behavior ($\mu_1 = \mu_2 = \mu_N$) when $\varphi = 90^o$ (see Fig. 1 (c) and Fig. 4).

Finally, the influence of the aspect ratio of fibers (l/d) is studied, l and d being the fiber length and diameter, respectively. In that case, the Halpin-Tsai micromechanical model for short-fiber FRP presented in [TuckerIII and Liang (1999)] is considered for that purpose. Fig. 9 (a) shows the influence of the fiber aspect ratio ($l/d = \{10, 20, 50, 100\}$) on the normal contact compliance, for a fixed volume fraction: $\bar{V}_\mathrm{f} = 0{,}30$. The lower values for l/d are considered, the lower normal compliance are obtained. These discrepancies are observed for a fiber alignment φ greater than 45^o. Fig. 9 (b) shows the tangential compliance. It can be observed how its values are not significantly affected by the fiber aspect ratio.

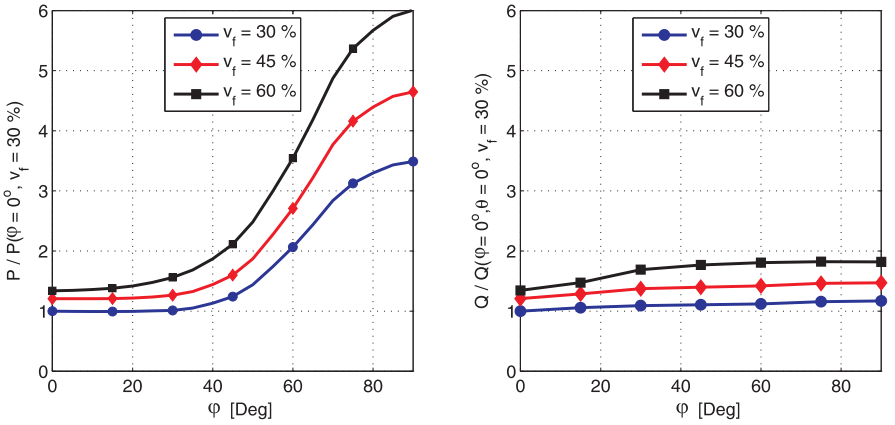

Figura 7: Normal (a) and tangential (b) contact compliance variation with the fiber orientation and fiber volume fraction.

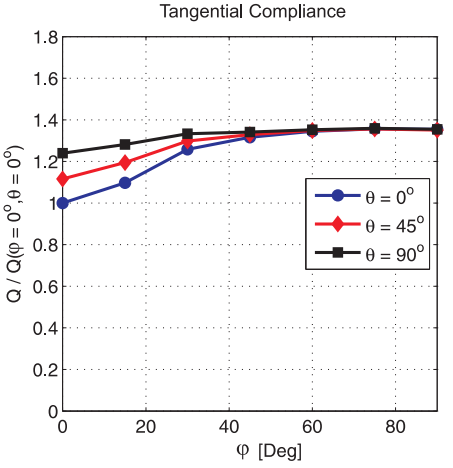

Figura 8: Tangential contact compliance variation with the fiber orientation and the sliding direction.

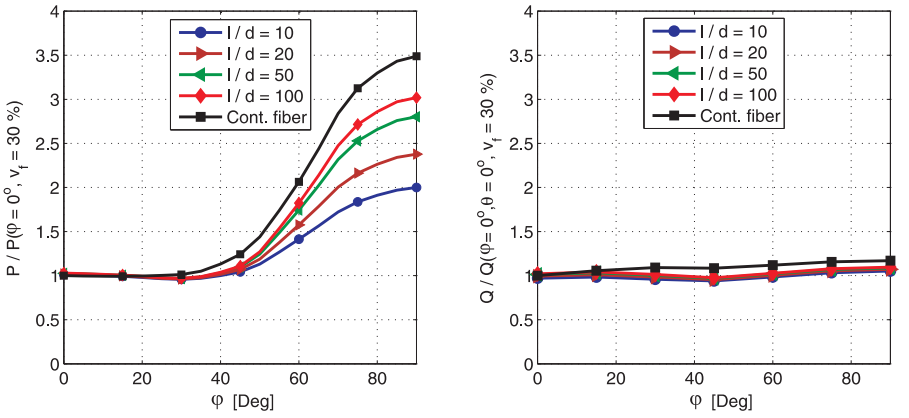

(a) (b)

Figura 9: Normal (a) and tangential (b) contact compliance variation with the fiber orientation.

9.3. FRP under fretting-wear conditions

The previous indentation problem is now studied under fretting wear conditions. The sphere is subjected to a normal displacement $g_{o,x_3} = -0{,}02\ mm$ and a repeated alternating tangential translational displacement of module $g_{o,t}$ (see Fig. 10), which forms an angle θ with axis x_1.

The carbon FRP considered is again IM7 Carbon/ $8551-7$, being the wear coefficients: $i_L = 5 \times 10^{-10}\ MPa^{-1}$, $i_T = 6{,}25 \times 10^{-10}\ MPa^{-1}$ and $i_N = 6{,}875 \times 10^{-10}\ MPa^{-1}$. In this fretting problem, the influence of the fiber orientation, the sliding direction, and the micromechanics of FRP (i.e. the fiber volume fraction or the aspect ratio of fibers) in the contact variables, are also studied.

The wear volume evolutions after 100,000 cycles are presented in Fig.11 for different fiber orientations and different fiber volume fractions: $\bar{V}_{\mathrm{f}} = \{0{,}30, 0{,}45, 0{,}60\}$, being the applied tangential load amplitude $g_{o,t} = 0{,}08\ mm$, and the tangential load orientation $\theta = 0^o$. The figure shows the enormous influence of the fiber orientation in the resulting wear volume (RWV). This influence is even more significant when the fiber volume fraction increases (see Fig.12).

The influence of the aspect ratio of fibers (l/d) in the resulting wear volume is also studied. Fig. 13 shows the influence of the fiber aspect ratio ($l/d = \{10, 20, 50, 100\}$) in the RWV, for a fixed volume fraction: $\bar{V}_{\mathrm{f}} = 0{,}30$. The lower values for l/d are considered, the lower RWV values are obtained. These discrepancies are observed

for a fiber alignment φ greater than 45^o, as it happens for the normal contact compliance. The RWV are not significantly affected by the fiber aspect ratio when φ is lower than 45^o.

Finally, Fig.14 shows the influence of the sliding direction (θ) on the resulting wear volume for a fiber volume fractions $\bar{V}_{\mathrm{f}} = 0{,}6$, and different fiber orientations. Examining Fig.14, it is found that the variation of the orientation of the sliding direction has and important effect on the magnitude of wear, when the fiber orientation is in the interval $[0^o, 45^o]$. For $\varphi = 90^o$, the RWV is not affected by θ, so an isotropic wear behavior is recovered, according with the proposed constitutive wear law.

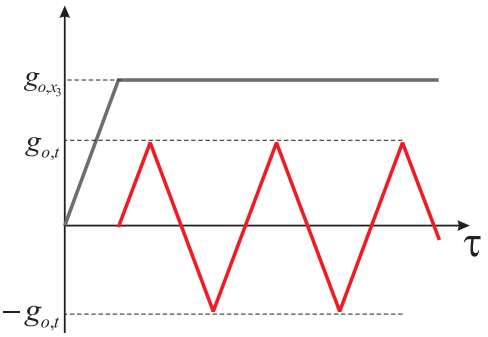

Figura 10: Cyclic tangential load.

10. Summary and conclusions

In the present work we propose new wear and friction constitutive laws and its numerical implementation, to study FRP materials under contact conditions. They are based on [Rodríguez-Tembleque, Abascal, and Aliabadi (2012a,b)], [Rodríguez-Tembleque, Buroni, Abascal, and Sáez (2013)] and [Rodríguez-Tembleque, Sáez, and Buroni (2013)], but the novelty with respect to these previous works is that the influence of the fiber orientation (φ) can be taken into account to compute the tribological properties on the surfaces (i.e. friction and wear coefficients). This allows us to have more realistic contact constitutive equations to simulate fiber-reinforced composite materials under frictional and wear conditions.

The methodology is based on the BEM, which proves to be a very suitable numerical method for this kind of tribological problems, obtaining a good approximation on contact and wear variables with a low number of elements, what makes faster the problem solution.

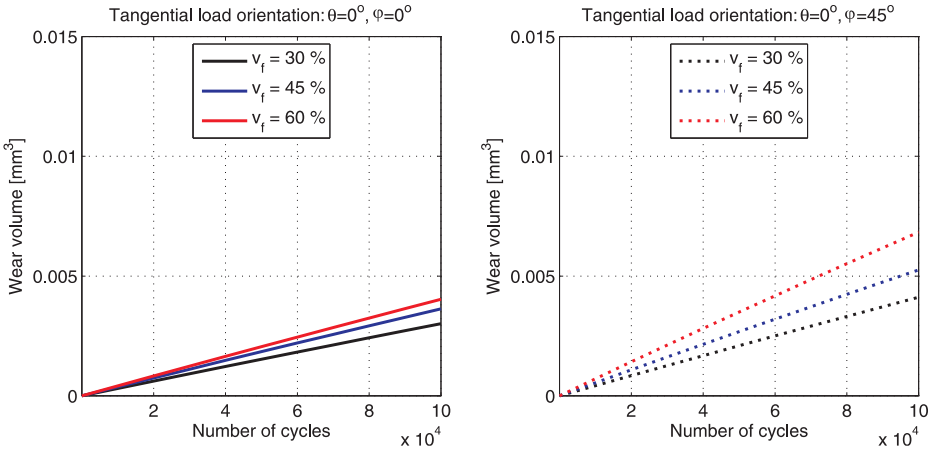

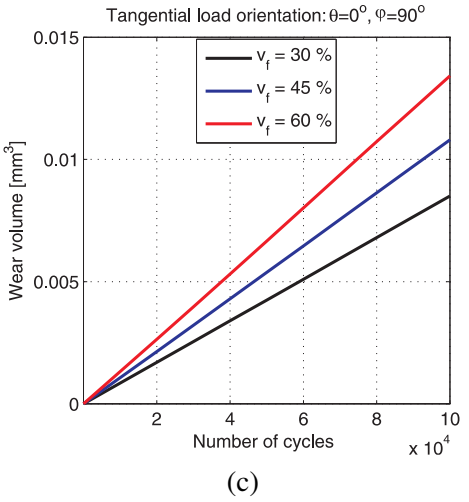

Figura 11: Wear volume evolution for different fiber volume fractions, and different fiber orientations: (a) $\varphi = 0^o$, (b) $\varphi = 45^o$, (c) $\varphi = 90^o$.

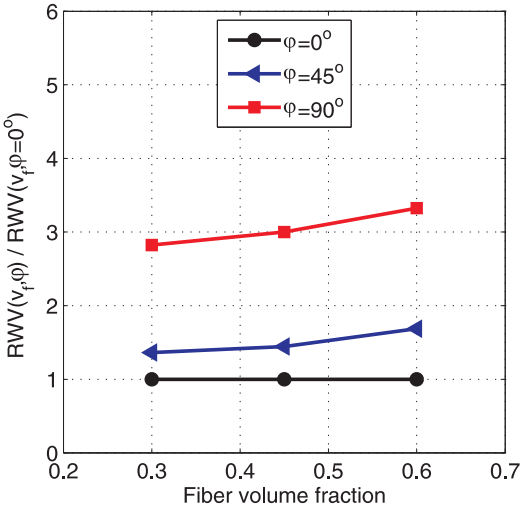

Figura 12: Influence of fiber orientation and fiber volume fraction on the resulting wear volume (RWV).

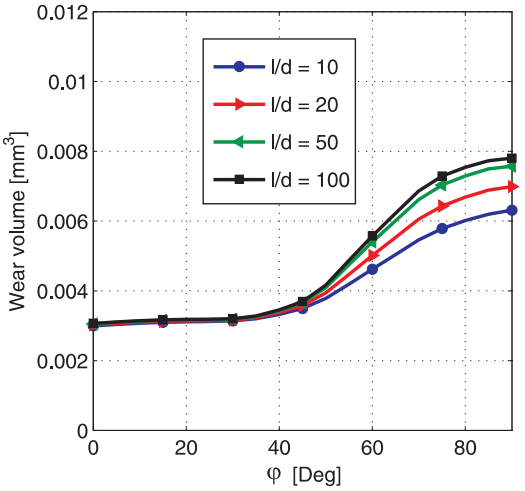

Figura 13: Influence of fiber orientation and fiber aspect ratio (l/d) on the resulting wear volume.

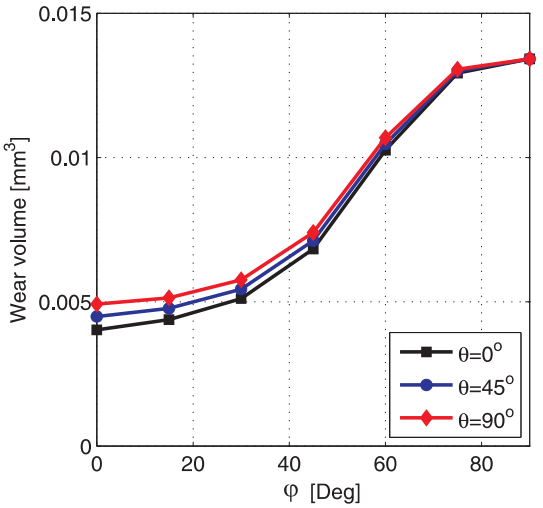

Figura 14: Influence of the fiber orientation and the sliding direction in the RWV.

Some contact and fretting wear studies on a carbon FRP are presented to show the importance of considering this new constitutive tribological properties. In other cases, we could over- or underestimate wear and contact magnitudes. For example, the normal contact compliance occurs for a normal fiber orientation ($\varphi = 90^o$), and high differences can be observed for φ greater than 45^o. In contrast, the tangential contact compliance presents the largest discrepancies for a fiber orientation in the interval $[0^o, 45^o]$.

Finally, it should be noted that the contact constitutive laws and the presented formulation should be extended not only to study aligned fiber reinforced composites in contact, but also to particle reinforced composite materials.

Acknowledgement: This work was funded by the *Ministerio de Ciencia e Innovacíon*, Spain, and by the *Consejería de Innovación Ciencia, y Empresa*, Junta de Andalucía (Spain), through the research projects: DPI2010-19331, DPI2013-43267-P and P12-TEP-2546, which were co-funded by the European Regional Development Fund (ERDF) (Fondo Europeo de Desarrollo Regional, FEDER).

Referencias

Aliabadi, M. H. (2002): *The Boundary Element Method Vol2: Applications in Solids and Structures*. John Wiley & Sons.

Araújo, F.; Gray, L. (2008): Evaluation of effective material parameters of cnt-reinforced composites via 3d bem. *CMES–Computer Modeling in Engineering and Sciences*, vol. 24, pp. 103–121.

Bagault, C.; Nélias, D.; Baietto, M. (2012): Contact analyses for anisotropic half space: Effect of the anisotropy on the pressure distribution and contact area. *J. Tribol.*, vol. 134, pp. 1–8.

Bagault, C.; Nélias, D.; Baietto, M.; Ovaert, T. (2013): Contact analyses for anisotropic half-space coated with an anisotropic layer: Effect of the anisotropy on the pressure distribution and contact area. *Int. J. Solids Struct.*, vol. 50, pp. 743–754.

Bagault, C.; Nélias, D.; Baietto, M.; Ovaert, T. (2013): Contact analyses for anisotropic half-space coated with an anisotropic layer: Effect of the anisotropy on the pressure distribution and contact area. *Int. J. Solids Struct.*, vol. 50, pp. 743–754.

Bank, L. (2006): *Composites for Construction - Structural Design with FRP Materials*. John Wiley & Sons.

Batra, R.; Jiang, W. (2008): Analytical solution of the contact problem of a rigid indenter and an anisotropic linear elastic layer. *Int. J. Solids Struct.*, vol. 45, pp. 5814–5830.

Buroni, F.; Sáez, A. (2013): Unique and explicit formulas for green's function in three-dimensional anisotropic linear elasticity. *Journal of Applied Mechanics*, vol. 80, pp. 051018.

Cavalieri, J.; Cardona, A. (2013): Three-dimensional numerical solution for wear prediction using a mortar contact algorithm. *Int. J. Numer. Methods Eng.*, vol. 96, pp. 467–486.

Cirino, M.; Friedrich, K.; Pipes, R. B. (1988): The effect of fiber orientation on the abrasive wear behavior of polymer composite materials. *Wear*, vol. 121, pp. 127–141.

Dong, L.; Atluri, S. N. (2012): Development of 3D T-Trefftz Voronoi Cell Finite Elements with/without Spherical Voids and/or Elastic/Rigid Inclusions for Micromechanical Modeling of Heterogeneous Materials. *CMC: Computers Materials and Continua*, vol. 29, no. 2, pp. 169–211.

Dong, L.; Atluri, S. N. (2013): SGBEM Voronoi Cells (SVCs), with Embedded Arbitrary-Shaped Inclusions, Voids, and/or Cracks, for Micromechanical Modeling of Heterogeneous Materials. *CMC: Computers Materials and Continua*, vol. 33, no. 2, pp. 111–154.

Friedrich, K. (1993): *Advances in composite tribology*. Elsevier.

Goda, T.; Vàradi, K.; Wetzel, B.; Friedrich, K. (2004): Finite element simulation of the fiber–matrix debonding in polymer composites produced by a sliding indentor: Part i – normally oriented fibers. *J. Compos. Mater.*, vol. 38, pp. 1583–1606.

Goda, T.; Vàradi, K.; Wetzel, B.; Friedrich, K. (2004): Finite element simulation of the fiber–matrix debonding in polymer composites produced by a sliding indentor: Part ii – parallel and anti-parallel fiber orientation. *J. Compos. Mater.*, vol. 38, pp. 1607–1618.

Graciani, E.; Mantic, V.; París, F.; Varna, J. (2009): Numerical analysis of debond propagation in the single fibre fragmentation test. *Compos. Sci. Technol.*, vol. 69, pp. 2514–2520.

Han, R.; Ingber, M.; Schreyer, H. (2006): Progression of failure in fiber-reinforced materials. *CMC–Computers, Materials, & Continua*, vol. 4, pp. 163–176.

Hopkins, D. A.; Chamis, C. C. (1988): *A Unique Set of Micromechanics Equations for High Temperature Metal Matrix Composites. In: Testing Technology of Metal Matrix Composites, ASTM STP 964,*. American Society for Testing and Materials.

Jacobs, O.; Friedrich, K.; Marom, G.; Schulte, K.; Wagner, H. D. (1990): Fretting wear performance of glass-, carbon-, and aramid-fibre/ epoxy and peek composites. *Wear*, vol. 135, pp. 207–216.

Jiang, W.; Batra, R. (2010): Indentation of a laminated composite plate with an interlayer rectangular void. *Compos. Sci. Technol.*, vol. 70, pp. 1023–1030.

Kaddour, A. S.; Hinton, M. J. (2012): Input data for test cases used in benchmarking triaxial failure theories of composites. *J. Compos. Mater.*, vol. 54, pp. 2295–2312.

Larsen, T.; Andersen, T. L.; Thorning, B.; Horsewell, A.; Vigild, M. (2007): Fretting wear performance of glass-, carbon-, and aramid-fibre/ epoxy and peek composites. *Wear*, vol. 262, pp. 1013–1020.

Lengiewicz, J.; Stupkiewicz, S. (2013): Efficient model of evolution of wear in quasi-steady-state sliding contacts. *Wear.*, vol. 303, pp. 611–621.

Leroux, J.; Nélias, D. (2011): Stick-slip analysis of a circular point contact between a rigid sphere and a flat unidirectional composite with cylindrical fibers. *Int. J. Solids Struct.*, vol. 148, pp. 3510–3520.

Lovell, M. (1998): Analysis of contact between transversely isotropic coated surfaces: development of stress and displacement relationships using fem. *Wear*, vol. 194, pp. 60–70.

Mallardo, V.; Alessandri, C. (2000): Inverse problems in the presence of inclusions and unilateral constraints: a boundary element approach. *Comput. Mech.*, vol. 26, pp. 571–581.

Ning, X.; Lovell, M. R. (2002): On the sliding friction characteristics of unidirectional continuous frp composites. *J. Tribol.*, vol. 124, pp. 5–13.

Ning, X.; Lovell, M. R.; Morrow, C. (2004): Anisotropic strength approach for wear analysis of unidirectional continuous frp composites. *J. Tribol.*, vol. 126, pp. 65–70.

Ning, X.; Lovell, M. R.; Slaughter, W. S. (2006): Asymptotic solutions for axisymmetric contact of a thin, transversely isotropic elastic laye. *Wear*, vol. 260, pp. 693–698.

Ohmae, N.; Kobayashi, K.; Tsukizoe, T. (1974): Characteristics of fretting of carbon fibre reinforced plastics. *Wear*, vol. 29, pp. 345–353.

Okada, H.; Fukui, Y.; Kumazawa, N. (2004): Homogenization analysis for particulate composite materials using the boundary element method. *CMES–Computer Modeling in Engineering and Sciences*, vol. 5, pp. 135–149.

Paczelt, I.; Kucharski, S.; Mróz, Z. (2012): The experimental and numerical analysis of quasi-steady wear processes for a sliding spherical indenter. *Wear.*, vol. 274-275, pp. 127–148.

Paczelt, I.; Mróz, Z. (2012): Solution of wear problems for monotonic and periodic sliding with *p*-version of the finite element method. *Comput. Meth. Appl. Mech. Eng.*, vol. 249-252, pp. 75–103.

Rodríguez-Tembleque, L.; Abascal, R. (2013): Fast fe-bem algorithms for orthotropic frictional contact. *Int. J. Numer. Meth. Eng.*, vol. 94, pp. 687–707.

Rodríguez-Tembleque, L.; Abascal, R.; Aliabadi, M. H. (2010): A boundary element formulation for wear modeling on 3d contact and rolling-contact problems. *Int. J. Solids Struct.*, vol. 47, pp. 2600–2612.

Rodríguez-Tembleque, L.; Abascal, R.; Aliabadi, M. H. (2011): A boundary element formulation for 3d fretting-wear problems. *Engng. Anal. Bound. Elem.*, vol. 35, pp. 935–943.

Rodríguez-Tembleque, L.; Abascal, R.; Aliabadi, M. H. (2012): Anisotropic fretting wear simulation using the boundary element method. *CMES–Computer Modeling in Engineering and Sciences*, vol. 87, pp. 127–155.

Rodríguez-Tembleque, L.; Abascal, R.; Aliabadi, M. H. (2012): Anisotropic wear framework for 3d contact and rolling problems. *Comput. Meth. Appl. Mech. Eng.*, vol. 241, pp. 1–19.

Rodríguez-Tembleque, L.; Buroni, F.; Abascal, R.; Sáez, A. (2013): Analysis of frp composites under frictional contact conditions. *Int. J. Solids Struct.*, vol. 50, pp. 3947–3959.

Rodríguez-Tembleque, L.; Buroni, F. C.; Abascal, R.; Sáez, A. (2011): 3d frictional contact of anisotropic solids using bem. *Eur. J. Mech. A. Solids.*, vol. 30, pp. 95–104.

Rodríguez-Tembleque, L.; Sáez, A.; Buroni, F. (2013): Numerical study of polymer composites in contact. *CMES–Computer Modeling in Engineering and Sciences.*, vol. 96, pp. 131–158.

Scholz, M.; Blanchfield, J.; Bloom, L.; Coburn, B.; Elkington, M.; Fuller, J.; Gilbert, M.; Muflahi, S.; Pernice, M.; Rae, S.; Trevarthen, J.; White, S.; Weaver, P.; Bond, I. (2011): The use of composite materials in modern orthopaedic medicine and prosthetic devices: A review. *Composites Science and Technology*, vol. 71, pp. 1791–1803.

Sharma, M.; Rao, I. M.; Bijwe, J. (2009): Influence of orientation of long fibers in carbon fiber-polyetherimide composites on mechanical and tribological properties. *Wear.*, vol. 267, pp. 839–845.

Stupkiewicz, S. (2013): An ale formulation for implicit time integration of quasi-steady-state wear problems. *Comput. Meth. Appl. Mech. Eng.*, vol. 260, pp. 130–142.

Sung, N. H.; Suh, N. P. (1979): Effect of fiber orientation on friction and wear of fiber reinforced polymeric composites. *Wear*, vol. 53, pp. 129–141.

Távara, L.; Mantic, V.; Graciani, E.; Canas, J.; París, F. (2010): Analysis of a crack in a thin adhesive layer between orthotropic materials: An application to composite interlaminar fracture toughness test. *CMES–Computer Modeling in Engineering and Sciences*, vol. 58, pp. 247–270.

Távara, L.; Mantic, V.; Graciani, E.; París, F. (2011): Bem analysis of crack onset and propagation along fiber-matrix interface under transverse tension using a linear elastic?brittle interface model. *Eng. Anal. Boundary Elem.*, vol. 35, pp. 207–222.

Tsukizoe, T.; Ohmae, N. (1983): Friction and wear of advanced composite materials. *Fibre Science and Technology*, vol. 18, pp. 265–286.

TuckerIII, C.; Liang, E. (1999): Stiffness predictions for unidirectional short-fiber composites: Review and evaluation. *Compos. Sci. Technol.*, vol. 59, pp. 655–671.

Vàradi; K., Nèder, Z.; Flöck, J.; Friedrich, K. (1998): Numerical and experimental contact analysis of a steel ball indented into a fibre reinforced polymer composite material. *Journal of Materials Science*, vol. 33, pp. 841–851.

Vàradi, K.; Nèder, Z.; Friedrich, K.; Flöck, J. (1999): Finite-element analysis of a polymer composite subjected to a ball indentation. *Compos. Sci. Technol.*, vol. 59, pp. 271–281.

Varna, J.; Paris, F.; del Cano, J. (1997): The effect of crack-face contact on fiber/matrix debonding in transverse tensile loading. *Compos. Sci. Technol.*, vol. 57, pp. 523–532.

Vishwanath, B.; Verma, A. P.; Rao, V. S. K. (1993): Effect of reinforcement on friction and wear of fabric reinforced polymer composites. *Wear*, vol. 167, pp. 93–99.

Wang, H.; Yao, Z. (2005): A new fast multipole boundary element method for large scale analysis of mechanical properties in 3d particle-reinforced composites. *CMES–Computer Modeling in Engineering and Sciences*, vol. 7, pp. 85–95.

Wang, H.; Z.H.Yao (2008): A rigid-fiber-based boundary element model for strength simulation of carbon nanotube reinforced composites. *CMES–Computer Modeling in Engineering and Sciences*, vol. 29, pp. 1–13.

Xiaoyu, J. (1995): Frictional contact analysis of composite materials. *Compos. Sci. Technol.*, vol. 54, pp. 341–348.